



# Numerical analysis of jet impingement cooling with elongated nozzle holes on a curved surface roughened with V-shaped ribs

Orhan Yalçınkaya<sup>1</sup> · Ufuk Durmaz<sup>1</sup>

Received: 25 July 2023 / Accepted: 27 January 2024 / Published online: 21 March 2024  
© The Author(s) 2024

## Abstract

Numerical studies were performed in this study to analyze the effect of dimensionless elongated injection holes ( $G/d=0.5, 2.0, 4.0, 8.0$ ) on heat and flow characteristics on rib-roughened surfaces with an array of inclined impingement jets. Experimental and numerical data from existing literature were used to validate the numerical solution procedure's heat transfer and flow characteristics in the semicircular test section. The turbulence equations were solved using the *SST k- $\omega$*  turbulence model by varying the Reynolds number from 5000 to 25,000. The curvature effect and staggered array pattern created an additional stagnation region between adjacent impinging jets on smooth surfaces, leading to a low heat transfer zone. Rectangular cross-sectional V-shaped ribs (*VSR*) were placed in regions where the stagnation point occurs to eliminate this disadvantage. The effect of different normalized rib heights ( $H_r/d=0, 0.2, 0.3, 0.4$ ) and rib angles ( $\alpha=30^\circ, 45^\circ, 60^\circ, 90^\circ$ ) on the curved surface was also investigated to increase convective heat transfer performance and achieve more homogenous heat transfer distribution by relatively reducing the effect of thermal stresses. Flow properties, area-averaged and local Nusselt number variations on smooth and ribbed surfaces, and the thermal performance criterion (*TPC*) were investigated in detail. The results indicated an increase in overall heat transfer and a more evenly distributed measurement region compared to the conventional (unextended jet and smooth surface) jet impingement configuration. The most significant heat transfer enhancement from combining the elongated jets with *VSR* was 47.23% at  $H_r/d=0.2$  by reducing the  $G/d$  to 0.5. In addition, the highest *TPC* was determined as 1.07 on the proposed model with  $G/d=2.0$  and  $H_r/d=0.2$  at  $Re=25,000$ .

**Keywords** Staggered nozzle design · Elongated jet hole · Roughened surface · V-shaped rib · Computational fluid dynamics

## List of symbols

		$\bar{h}$	Mean convective heat transfer coefficient ( $\text{W m}^{-2} \text{K}^{-1}$ )
C-CRV	Counter-clockwise rotating vortex	$H$	Orifice surface-target surface distance (m)
CFD	Computational fluid dynamics	$H/d$	Dimensionless orifice plate-to-target surface spacing
CJIC	Conventional jet impingement cooling	$H_r$	Rib height (m)
CRV	Clockwise rotating vortex	$H_r/d$	Rib height to jet diameter ratio
$d$	Jet diameter (m)	$I$	Turbulence intensity
$G$	Nozzle-target surface spacing (m)	$k$	Thermal conductivity ( $\text{Wism}^{-1} \text{K}^{-1}$ )
GCI	Grid Convergence Index	$K$	Kelvin scale of thermodynamic temperature
$G/d$	Dimensionless target surface-to-nozzle spacing	$Nu_{ave}$	Mean Nu number
$G_s$	Row spacing in the spanwise direction (m)	$Re$	Jet Reynolds number
$h$	Convective heat transfer coefficient ( $\text{W m}^{-2} \text{K}^{-1}$ )	$s/d$	Longitudinal central plane
		SIMPLEC	Semi-Implicit Method for Pressure Linked Equations-Consistent
		SST	Shear stress transport
		TPC	Thermal performance criterion
		$V$	Average air velocity ( $\text{m s}^{-1}$ )
		$W_t$	Target surface width (m)
		$x$	Coordinate in the flow direction
		$x/d$	Dimensionless streamwise distance

✉ Orhan Yalçınkaya  
orhanyalcinkaya@sakarya.edu.tr

Ufuk Durmaz  
udurmaz@sakarya.edu.tr

<sup>1</sup> Faculty of Engineering, Mechanical Engineering Department, Sakarya University, 54050 Sakarya, Turkey

$y^+$	Normalized wall distance
$z$	Coordinate perpendicular to $x$
$T_w$	Wall temperature (K)
$T_\infty$	Air temperature (K)

#### Subscripts and superscripts

ave	Average
r	Rib
j	Jet

#### Symbols

$\alpha$	Rib angle ( $^\circ$ )
$\rho$	Air density ( $\text{kg m}^{-3}$ )
$\mu$	Dynamic viscosity (Pa s)
$\Gamma$	Diffusion coefficient ( $\text{m}^2 \text{s}^{-1}$ )

## Introduction

Recently, operating temperatures in gas turbines have increased to satisfy the need for greater power output and enhanced thermal efficiencies. The leading edges of gas turbine blades are directly subjected to high-temperature combustion gases, reaching temperatures of several thousand degrees. This can cause significant thermal stress and damage to the blades, ultimately leading to reduced performance and lifespan of the turbine. Materials that can withstand higher temperatures are used to mitigate this, and advanced cooling techniques are implemented. Additionally, advanced cooling techniques, such as film and internal cooling, can help protect the blades from hot combustion gases. Recently, there has been an increasing trend in the investigation and development of jet impingement cooling.

Many factors can affect the performance of jet impingement cooling, an internal cooling method that involves directing high-speed coolant jets onto a surface. Some key parameters that can affect the performance of jet impingement cooling include jet Reynolds number ( $Re$ ), injection hole-to-surface angle [1] and distance [2–4], coolant temperature, and impingement plate-target surface distance [5, 6]. Also, elongated jets can directly influence a system's thermal and hydraulic performance [7–9].

Demir et al. [10] investigated the flow field and heat transfer of swirling impinging jets at low nozzle-plate distances, considering three cases with six turbulence models on a flat plate. At distances below  $G/d < 1.00$ , negative pressure regions occurred for all Reynolds numbers, with the magnitude increasing as the Reynolds number increased and  $G/d$  decreased. In addition, El-Wafa et al. [11] experimentally investigated the impact of a movable air jet on heat transfer characteristics over a flat plate, comparing it with a fixed nozzle. Results show that the movable nozzle is more effective in reducing temperature variation, leading to enhanced heat transfer uniformity

more than the fixed nozzle, with maximum improvements of 75%, 42%, 39%, and 43% at different  $G/d$  ratios. Fenot et al. [12] examined the high relative curvature effect on heat transfer under an array of impinging jet flow over a curved semi-cylindrical surface by changing parameters such as jet diameter, the distances of adjacent jets, and the jet outlet-target surface. Using a linear regression method, they experimentally determined adiabatic wall temperatures and local heat transfer coefficients. In general, they found that the high relative curvature considerably affects the heat transfer on a concave surface. They also determined that the local heat transfer dissipation on a concave surface exhibits similar characteristics to that on a flat plate. Lyu et al. [13] investigated the variation of heat transfer coefficient and adiabatic wall temperature on a concave surface with four different curvature ratios in a single-row chevron-nozzle impinging jet. They conducted an experimental investigation for several jet-target plate distances under different  $Re$  numbers. As a result, they stated that the semi-cylindrical concave surface showed the highest heat transfer performance in the mid-plane. The results indicated that employing a chevron nozzle leads to approximately a 20–30% increase in the longitudinally mean Nusselt number ( $Nu$ ) compared to a round nozzle. Yang et al. [14] evaluated the effect of designing geometric parameters such as inter-jet distance, jet inclination angle, jet-target surface distance, and jet diameter on the sonic impingement jet's heat and flow characteristics of a curved surface of a NACA0015 airfoil. According to the results, heat transfer performance could be improved by determining the optimum structural parameters. Also, the flow properties of multi-impinging jets are substantially affected by the inclination angle and the spacing between adjacent jets. Jung et al. [15, 16] conducted a study comparing heat transfer characteristics of two different jet configurations: a standard  $3 \times 5$  jet arrangement and an inclined jet array. According to their findings, the inclined array jet arrangement performed better regarding heat transfer characteristics. Heo et al. [17] performed a study to optimize the placement of inclined impinging jets. They found that the injection hole angle that resulted in the highest cooling effectiveness was around 60 deg on a concave surface. Qui et al. [18] investigated the impact of jet arrangements on fluid flow and heat transfer characteristics for three array jets impinging onto a curved surface with varying jet-to-jet spacing and Reynolds numbers. The findings revealed that both inline and staggered arrangements significantly enhance heat transfer uniformity compared to an array jets case, with improved performance observed when side array jets are positioned further from the middle array.

Another concern of impinging jet cooling is improving the heat transfer uniformity. This is because, in some cases, the heat transfer rate may be non-uniform, leading to hot

spots or cold spots on the impingement surface. Various factors, including the non-uniform distribution of the impinging jet or the non-uniform heat flux on the surface, can cause non-uniformity in heat transfer. To enhance heat transfer homogeneity, the impinging jets need to be distributed uniformly on the confinement plate, and the heat transfer dissipation on the target surface needs to be controlled with ribs [19–22], pins [23, 24], grooves [25], dimples [26–28], baffles [29], waveforms [30], etc. In addition to these methods, swirling jets [31] and pulsating jets [32] can be preferred for homogeneous temperature distribution.

When the jet flow hits the surface, it creates a stagnation zone where the fluid velocity is reduced to zero. This region experiences a significantly high local heat transfer coefficient due to the intense turbulence and mixing of the fluid. However, the local heat transfer degrades rapidly away from the stagnation zone as the fluid spreads out and its velocity decreases. This means that the cooling effect of the impinging jet is limited to a relatively small area around the stagnation zone. In the case of a row of jets, the cooling effect is more uniform but still limited to the area directly under the jets. Multiple rows of jets can be used to improve the cooling performance, with each row targeting a different surface area.

Also, other cooling techniques, such as rib turbulators, can be synchronized with an impinging jet. The use of ribbed surfaces in jet impingement has been extensively studied, both experimentally and numerically. Different types of rib geometries, such as circular, rectangular, and triangular ribs, as well as different rib heights and spacings, have been investigated. Yan et al. [33] experimentally investigated the impact of *VSR* deg (45, 60, and 90) on local heat transfer distributions on a flat surface using the crystal thermography technique in a conventional jet impingement cooling scheme. In addition, three different normalized injection holes-target surface spacings ( $H/d=3.0, 6.0, 9.0$ ) were examined. The best heat transfer performance was achieved using *VSR* at an angle of 45 deg at  $H/d=3.0$ . Katti and Prabhu [34] experimentally investigated heat transfer dissipation on a flat surface according to parameters such as the height and width of the ribs and the distance between the ribs. The heat transfer in the stagnation region was higher on the roughened surface than on the smooth surface. Caliskan and Baskaya [35] conducted a study to examine the heat transfer and flow characteristics on a flat surface roughened with *VSR* at different dimensionless jet-target plate ratios ( $H/d=3.0$  and  $12.0$ ). At low  $H/d$  ratios, turbulent kinetic energy was higher on *VSR*-roughened surfaces. In addition,  $Nu$  numbers on ribbed surfaces were higher than on smooth surfaces. In a similar study, Caliskan and Baskaya [36] measured heat transfer using a thermal infrared camera on a surface with *VSR* and convergent-divergent ribs for variable rib heights under a conventional impinging jet. The mean  $Nu$

number on the *VSR*-roughened surface increased from 4% to 26.6% over the smooth surface. Tong et al. [20] numerically examined four different target surface configurations, such as smooth, round pinned, square pinned, and cambered ribbed surfaces, considering the real turbine operating conditions in the multiple array jet impingement model. In particular, they determined that the cambered ribbed elements could improve the average  $Nu$  number by up to 62.6% compared to the smooth surface. Rasheed et al. [37] investigated the heat transfer characteristics of a single jet flow over a heated surface with detached ribs. Various rib configurations were explored using the generalized  $k-\omega$  turbulence model, varying width, height, clearance, pitch, and radial distance. The study revealed that the nozzle's proximity to the impingement plate is crucial for achieving maximum heat transfer.

Compared to similar studies, the innovation in this work lies in investigating the effects of dimensionless elongated injection holes on heat and flow characteristics over rib-roughened surfaces with inclined impingement jets. For example, in an elongated jet-impinging model, Tepe et al. [38] experimentally examined the heat transfer properties for a constant rib angle ( $\alpha=90^\circ$ ) on a flat surface. In the present study, the effects of ribs with variable heights and different angles on a concave surface in accordance with the leading edge of gas turbine blades on both heat and flow characteristics were examined in detail. Moreover, in a numerical study by Tepe [9], dead flow zones were observed on a smooth concave surface, especially in the last jet regions and between elongated adjacent jets. In this study, *VSRs* were mounted on a concave surface to minimize this negative effect, and the results were compared with smooth surface models. In addition, Yan et al. [33] experimentally investigated the impact of *VSR* deg on local heat transfer distributions on a flat surface in a conventional (without elongated jet holes) jet impingement cooling scheme. The current study examined the elongated jet effect on a concave surface roughened with *VSRs*.

The purpose of this study is to investigate the effects of dimensionless elongated injection holes on heat and flow characteristics over rib-roughened surfaces with inclined impingement jets and assess the feasibility of the proposed designs. The study also explores using *VSR* to address low heat transfer zones and improve the overall heat transfer efficiency on a curved surface. Combining elongated jets and ribs aims to achieve a more uniform heat transfer distribution and enhance the cooling system's performance. There is no existing literature study that investigates the use of a concave surface in conjunction with elongated jet holes and ribs. Different normalized injection hole-to-target surface distances ( $0.5 \leq G/d \leq 8.0$  for  $H/d=8.0$ ), normalized *VSR* heights ( $H_r/d=0, 0.2, 0.3, 0.4$ ), rib angles ( $\alpha=30^\circ, 45^\circ, 60^\circ, 90^\circ$ ) and  $Re$  numbers ( $5000 \leq Re \leq 25,000$ ) are investigated with *SST*  $k-\omega$  turbulence model in commercial ANSYS Fluent.

Also, the mean and local  $Nu$  numbers, flow features, and  $TPC$  are studied to elucidate the effects of  $G/d$  on a rib-roughened semicircular curved surface. Finally, the proposed model is compared to the standard jet-impinging design to determine the influence of the elongated nozzle holes and  $VSR$ -roughened surfaces. Furthermore, the results of this investigation will provide insight into whether the combination of elongated jets and ribs can be an effective method for enhancing heat transfer uniformity in gas turbine components.

## Model description

Figure 1 provides a detailed view of the proposed model for a rib-roughened surface, including perspective and left-side views. In addition, the figure provides details on the configuration and size of the rib-roughened surface. The semicircular concave duct has a hydraulic inlet diameter measuring 32.5 mm. Airflow exits the jet and impinges the test plate perpendicularly. After impinging on the surface, the airflow discharges from the concave duct in the direction of flow, typically along the  $x$ -axis. The jets, which are elongated toward the target surface, have a diameter of  $d=5$  mm and a wall thickness of  $t/d=0.2$ . The  $3 \times 5$  staggered jet arrangement

was created on the confinement plate. The jet rows on the orifice surface are positioned at an angle of 25 deg with respect to the  $z$ -axis. Inclined nozzles are assembled at  $s/d=0$  and  $\pm 2.6$ . The spacing between consecutive rows of holes in the streamwise direction is  $6d$ . The measurement region on the target surface is determined as  $\pm 60$  deg in the  $s$ -direction, which is suitable for the experimental study [16].

Two different normalized distances of the orifice-to-target surface ( $H/d=1.0$  and  $H/d=8.0$ ) were investigated. While  $H/d=1.0$  was used only to validate the numerical solution procedure, the  $H/d=8.0$  ratio was considered constant in all other analyses. Also, the test plate was roughened with  $VSR$ . Overall, the combination of the jet diameter, jet angle, rib layout, and distance between the nozzles was chosen to optimize the heat transfer efficiency and temperature uniformity. The geometric parameters, such as the height and angle of the rib, can significantly affect the test plate's heat transfer distribution and temperature uniformity by influencing the turbulence and fluid flow around the ribs. A study has shown that a sweep angle of around 45 deg results in the best heat transfer enhancement [33]. At this angle, the ribs create vortices that promote mixing and reduce the thickness of the boundary layer, resulting in increased heat transfer. For this reason,

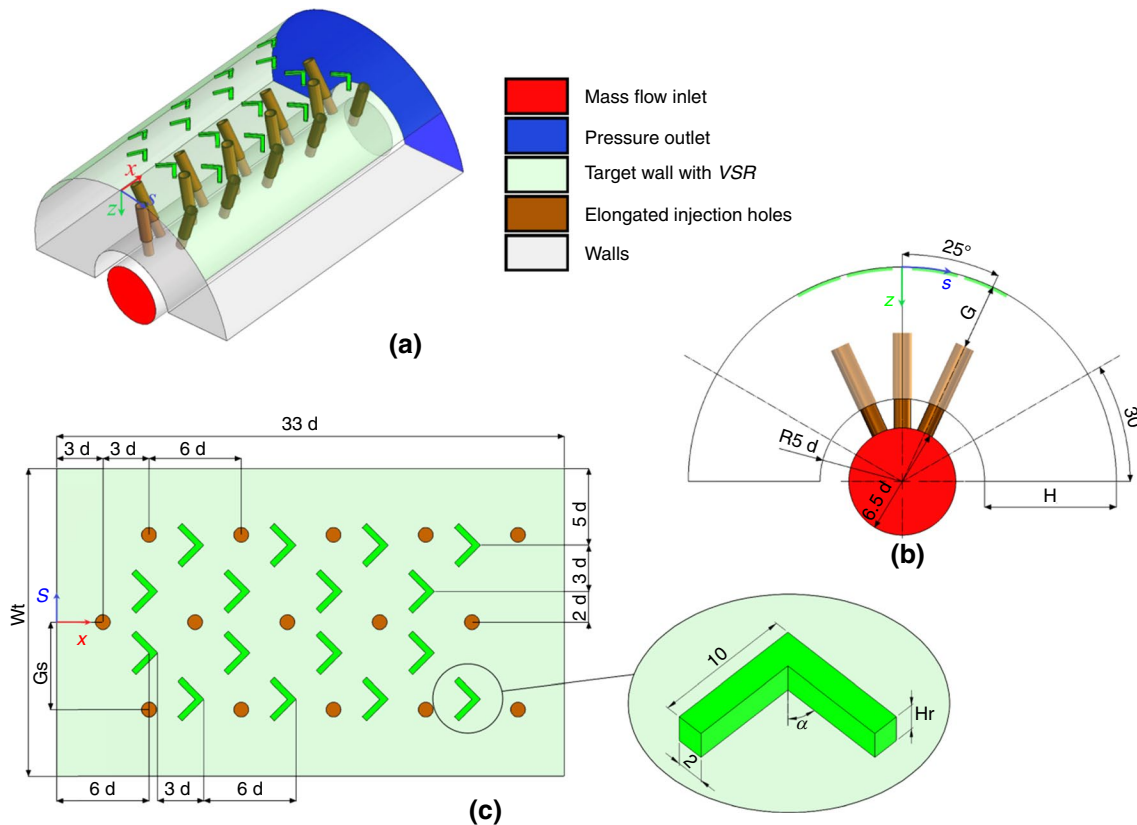


**Fig. 1** Drawings and dimensions of the fluid domain, **a** 3-D image, **b** cross-sectional front view, **c** nozzle and rib configuration of the physical model

45 deg-*VSR* was preferred on the relevant surface in this study.

Simulating turbulence flow regimes ( $5000 \leq Re \leq 25,000$ ) was conducted for physical models using computational fluid dynamics (*CFD*) methods. The values of  $G/d$  examined were 0.5, 2.0, 4.0, and 8.0 for  $H/d=8.0$ . Equations (1) and (2) describe relationships between the impingement surface-to-target surface distance ( $H$ ), jet diameter ( $d$ ), target surface width ( $W_t$ ), and row spacing ( $G_s$ ). These equations can be used to calculate the  $W_t$  and  $G_s$  for a given  $H$  and  $d$ .

$$W_t = 2.094H + 10.472d \tag{1}$$

$$G_s = 0.436H + 2.182d \tag{2}$$

### Governing equations

In this study, the ANSYS Fluent software, which helps optimize the cooling system’s design, was utilized to examine the flow and heat transfer distributions in the physical model and solve the Reynolds-averaged Navier–Stokes (*RANS*) equations with the *SST k- $\omega$*  turbulence model developed by Menter [39, 40]. The impingement jet flow and convection heat transfer characteristics are calculated using governing equations, including the equations of continuity, momentum, and energy in steady-state conditions presented below as Eqs. (3)–(5), respectively.

$$\frac{\partial(\rho u_i)}{\partial x_i} = 0 \tag{3}$$

$$\frac{\partial(\rho u_i u_j)}{\partial x_i} = -\frac{\partial P}{\partial x_i} + \frac{\partial}{\partial x_i} \left[ \mu \left( \frac{\partial u_i}{\partial x_j} \right) + \frac{\partial u_j}{\partial x_i} - \frac{2}{3} \delta_{ij} \frac{\partial u_i}{\partial x_j} \right] + \frac{\partial}{\partial x_i} \left( -\overline{\rho u_i' u_j'} \right) \tag{4}$$

$$\frac{\partial}{\partial x_i} \left[ u_i (\rho E + P) \right] = \frac{\partial}{\partial x_j} \left[ \left( k + \frac{c_p \mu_t}{Pr_t} \right) \frac{\partial T}{\partial x_j} + u_i (\tau_{ij})_{\text{eff}} \right] + S_h \tag{5}$$

When dealing with low mass flow rates, laminar flow is often required. However, it is necessary to calculate the turbulence component to predict jet impingement. The boundary layer at the stagnation region is extremely thin, and the flow features within the viscous sub-layer significantly impact the heat transfer on the target wall. To ensure accurate predictions of the impinging jet in this study, the *SST k- $\omega$*  model was utilized because predicting the flow in the viscous sub-layer is well-known due to its diffusion-based calculations. *SST k- $\omega$*  turbulence model uses governing equations, expressed as Eq. (6) and Eq. (7), in a steady state condition.

$$\frac{\partial(\rho k u_i)}{\partial x_i} = \frac{\partial}{\partial x_j} \left( \Gamma_k \frac{\partial k}{\partial x_j} \right) + G_k - Y_k + S_k \tag{6}$$

$$\frac{\partial(\rho w u_i)}{\partial x_i} = \frac{\partial}{\partial x_j} \left( \Gamma_w \frac{\partial w}{\partial x_j} \right) + G_w - Y_w + D_w + S_w \tag{7}$$

Jet Reynolds number is used to characterize the flow regime of a fluid jet and is defined in Eq. (8) as:

$$Re = \frac{\rho V d}{\mu} \tag{8}$$

where  $V$  represents the average flow velocity within the nozzle, the other variables are the process fluid density ( $\rho$ ) and dynamic viscosity ( $\mu$ ).

The local heat transfer coefficient ( $h$ ) is a measure of the rate at which heat is transferred from a fluid to a solid surface and is described in Eq. (9). Also, it is influenced by the flow regime of the fluid jet, the jet’s diameter, the distance between the jet and the surface, and the surface roughness and temperature.

$$h = \frac{q''}{T_w - T_\infty} \tag{9}$$

The term  $q''$  refers to the heat flux, which measures the heat transfer rate per unit area. The temperatures of the fluid ( $T_\infty$ ) and the wall ( $T_w$ ) are also important variables in this context. Specifically,  $T_\infty$  represents the temperature of the fluid far away from the wall while  $T_w$  is the wall’s temperature. Besides, the average Nusselt number is calculated using Eq. (10).

$$Nu_{\text{ave}} = \frac{\bar{h} d}{k} \tag{10}$$

where  $\bar{h}$  describes the overall heat transfer rate per unit area of the target surface and is calculated by averaging the local heat transfer coefficients over the entire measurement region.

The turbulence intensity ( $I$ ) describes the ratio of the turbulent velocity fluctuations to the mean velocity of the fluid. It can be calculated at the inlet and outlet sections of a cooling system by Eq. (11).

$$I = 0.16Re^{-1/8} \tag{11}$$

### Numerical analysis

Numerical simulations were conducted using ANSYS Fluent, and the physical model was verified through experimental results obtained by Jung et al. [16]. A comparison is presented between the outcomes of commonly



used viscous models to determine the best turbulence model for impingement jets with elongated holes and ribs.

## Numerical solution procedure

It is important to note that the choice of boundary conditions can significantly impact the accuracy of the numerical solution and the results. Initial boundary conditions of the computational domain are shown in Table 1. The symmetry plane is defined on the middle axis to reduce computational costs. In addition, the process fluid with a temperature of  $T_{\infty} = 47$  °C enters a circular inlet section. Also, the target surface is kept at a temperature of  $T_w = 27$  °C. The non-slip and adiabatic wall is determined as the boundary condition for the remaining wall portion aside from the 60° target surface. The examination is carried out under three different mass flow rates. The turbulent inlet intensity of the process fluid in the concave channel is set as 4.55%, 3.95%, and 3.73% for  $Re = 5000$ , 15,000, and 25,000, respectively. The static pressure of 101.325 kPa is applied for the outlet section of the fluid domain. While the non-slip boundary condition is implemented for the entire calculation area, the adiabatic wall surface boundary condition is defined for all walls except the measurement region (target surface).

Based on the specified mass flow rates, Reynolds numbers were determined to be higher than  $4 \times 10^3$  and developed fully turbulent flow [41] in the concave duct. SIMPLEC algorithm was employed to solve the pressure–velocity coupling. A second-order upwind scheme was utilized for discretizing spatial derivatives in the partial differential equations. When the scaled residuals reached  $10^{-5}$ , the solution was considered converged, and the computations were completed in this study. The thermophysical properties of the coolant air are given in Table 2 [42].

## Assessment of grid independence

The mesh structure plays a critical role in the accuracy and solution of the numerical model. It is important to ensure the mesh is fine enough in regions where the solution is expected to be highly sensitive to the grid size, such as the target surface, elongated jets, and wall jet region. This is accomplished by

creating more dense grid cells in these regions, as shown in Fig. 2. A finer mesh can capture more details of the flow and heat transfer phenomena, which leads to more accurate results. However, a fine mesh also increases the computational cost, so balancing accuracy and computational cost is essential.

Figure 2 provides a detailed overview of the grid structure. Polyhedral finite elements, preferred in this study, are a type of mesh structure commonly used in engineering applications. The polyhedral elements can adapt to the model's geometry, allowing for more accurate results and reduced computational costs. These elements are particularly useful for complex geometries, such as the concave duct with ribs in the proposed physical model. Furthermore, the figure also includes colored representations of named selections.

Mesh independence study typically involves simulations with different mesh structures or grid sizes and comparing the results. Table 3 shows the results of grid structures examined at  $Re = 25,000$  and  $H/d = 8.0$  for  $G/d = 4.0$ ,  $H_r/d = 0.2$ .

Grid Convergence Index ( $GCI$ ) with Richardson extrapolation [43, 44] was used to estimate the discretization error in the numerical calculations. The mean  $Nu$  number was quantitatively assessed using three different mesh structures. Relative errors in  $GCI_{23}$  and  $GCI_{12}$  were calculated as 1.07% and 0.19%, respectively. Furthermore, the relative error between the extrapolation and fine grid was only 0.15%. The value of  $\frac{GCI_{21}}{r^p GCI_{32}}$  was found to be 1.0071, indicating that it is in the asymptotic range of convergence ( $\frac{GCI_{21}}{r^p GCI_{32}} = 1$ ). Based on these results, it can be concluded that further refinement of the grid is unnecessary, as the reduction in error would be minimal compared to the computational cost of further grid refinement. For this reason, the Fine (1) grid structure was preferred in all computations.

**Table 1** The computational domain initial boundary conditions

The temperature of the fluid entering the process	47	°C
A fixed wall temperature for the measurement region	27	°C
Adiabatic and non-slip condition on the walls	–	–
Static pressure at the outlet section	101.325	kPa
Inlet mass flow rates for symmetric models at $Re = 5000$ , 15,000, and 25,000	$2.88 \times 10^{-3}$ $8.64 \times 10^{-3}$ $14.4 \times 10^{-3}$	$\text{kg s}^{-1}$
Inlet turbulent intensities at $Re = 5000$ , 15,000, and 25,000	4.55, 3.95, 3.73	%

**Table 2** Thermophysical properties of coolant air [42]

	Density/kg $\text{m}^{-3}$	Specific heat value/J $\text{kg}^{-1} \text{K}^{-1}$	Kinematic viscosity/ $\text{m}^2$ $\text{s}^{-1}$	Thermal conductivity coefficient/ $\text{W}$ $\text{m}^{-1} \text{K}^{-1}$
Air	1.094	1007.4	$1.6343 \times 10^{-5}$	0.027801

**Fig. 2** Mesh detail of the computational domain for  $H/d=8.0$  and  $G/d=2.0$  with ribbed surface

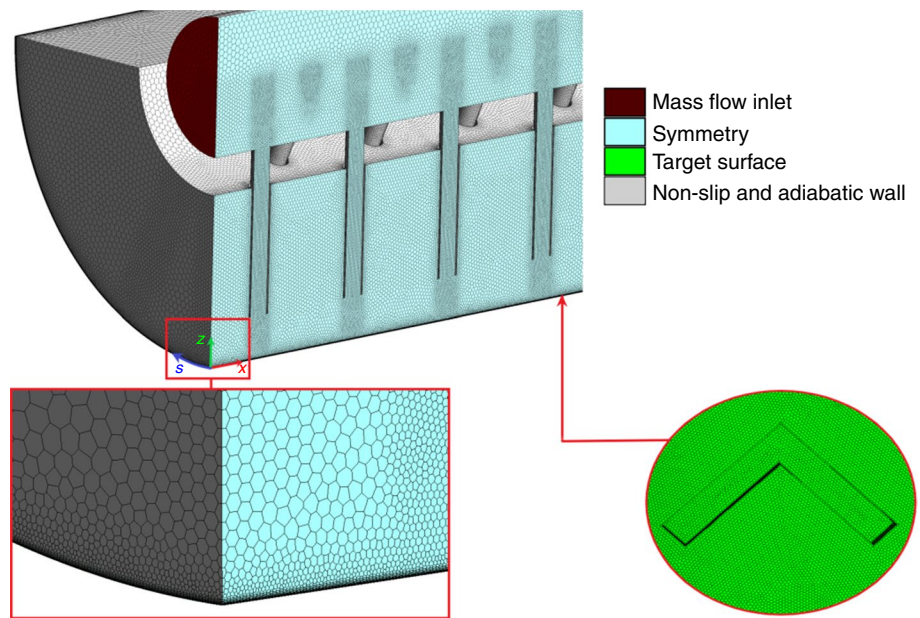


**Table 3** Grid independence behavior on a ribbed surface

Mesh	Coarse (3)	Medium (2)	Fine (1)	Extrapolation
Element	$3.16 \times 10^6$	$5.52 \times 10^6$	$7.23 \times 10^6$	
$y^+$	1.22	0.94	0.92	
$Nu_{ave}$	65.19	67.93	68.42	68.52
Relative error	1.07%	0.19%	0.15%	

Moreover, the numerical result of the velocity vector field on  $x/d=3.0$  obtained using Fine (1) under the same conditions ( $G/d=1.0$  and smooth surface at  $H/d=1.0$ ) was compared with the result of Jung et al. [16]. As clearly seen in Fig. 3, primary vortices were formed near the impingement point of the jets ( $s/d \cong -1.5$ ), where the fluid flow is

highly turbulent due to the interaction of the fluid flow with the surface and the jet for both studies. Likewise, secondary vortices were formed in almost the same location, farther away from the impingement point ( $s/d \cong -6.0$ ), due to the instability and turbulence of the primary vortices. Therefore, it is also inferred that the mesh procedure agreed well with the result in the literature.

**Verification of computational solution approach**

Finding a turbulence model that can accurately analyze every physical problem is difficult. Therefore, it is necessary to carefully compare the results from different solution procedures to select the most appropriate model for a particular problem. In summary, verification of computational

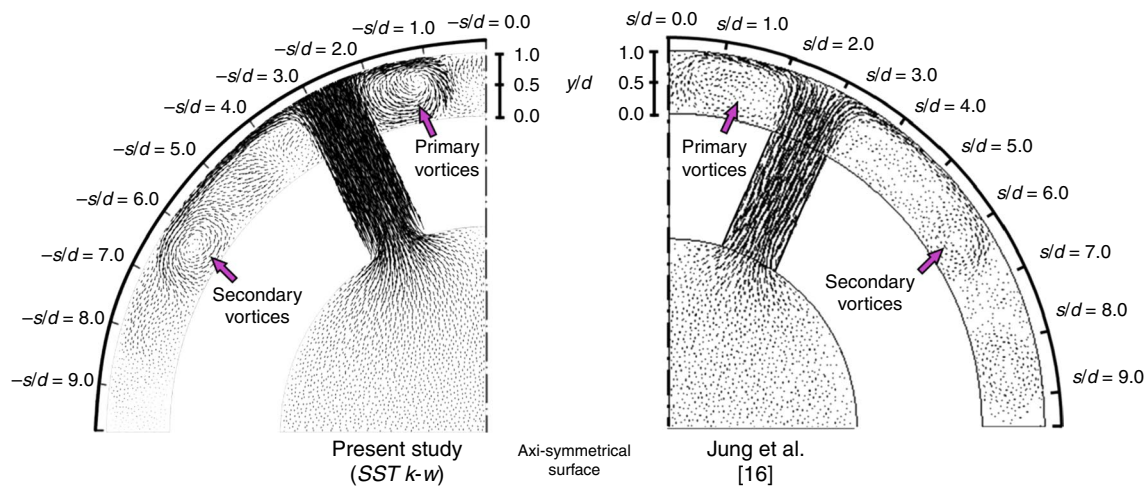


**Fig. 3** Velocity vector plot comparison of numerical study and Jung et al.'s [16] study

solution methodology and turbulence model selection is an essential step in the numerical simulation process to ensure the results are accurate and reliable. Therefore, the local  $Nu$  number distribution results along the flow direction of the turbulence models commonly used in the literature in the impinging jet cooling method are presented in Fig. 4a. In addition, the local  $Nu$  distribution contour on the smooth concave surface at  $H/d=1.0$  and  $Re=5000$  for  $G/d=1.0$  is also compared in Fig. 4a with the experiment by Jung et al. [16] to validate the numerical solution approach. Moreover, the area-averaged  $Nu$  number change for investigated turbulence models depending on the  $Re$  numbers is given in Fig. 4b.

Turbulence models tend to overestimate experimental results, especially in impingement regions. On the other hand, the  $SST\ k-\omega$  model exhibits a reasonable prediction with the experimental values for axial changing of the local  $Nu$  number, as illustrated in Fig. 4a. This is supported by a better agreement of the local  $Nu$  distribution on the target surface with the experimental results [16] simultaneously. The figure clearly indicates that the  $SST\ k-\omega$  model predicted well the  $Nu$  contour of the experimental study. Besides, the area-averaged  $Nu$  numbers for the relevant surface were obtained by averaging the local estimations within the  $-4.0 \leq s/d \leq 4.0$  and  $0 \leq x/d \leq 33$ . The maximum deviation of 9.4% was calculated in the prediction of the average  $Nu$  numbers. The hydraulic performance criterion was also considered to validate the numerical procedure further. Therefore, the pressure drop was also studied. As shown in Fig. 5, the solution procedure reveals Tepe's numerical pressure drop data [9] with a maximum deviation of 10.6% at  $H/d=8.0$  under different  $Re$  numbers. Consequently, the solution methodology was adopted for all subsequent computations, and the findings were examined in detail.

## Result and discussion

V-shaped ribs were applied in the present study to decrease the low heat transfer region on smooth surfaces. However, heat transfer performance significantly varied with the angle of the ribs ( $\alpha$ ). Therefore, it is better first to discuss how to decide the collocation of impingement holes and  $VSRs$  to achieve the best heat transfer performance. Figure 6a shows the mean  $Nu$  number increased more on the surface with 45 deg  $VSRs$  at  $Re=25,000$  for  $H/d=0.2$  and  $H/d=8.0$  and compared to the smooth surface, like in the literature [33]. Also,  $VSR$  at an angle of 45 deg helped distribute the flow more evenly and effectively across the surface, preventing areas of low heat transfer, as shown in Fig. 6a. For this reason, 45 deg- $VSRs$  were investigated on the target surface in detail.

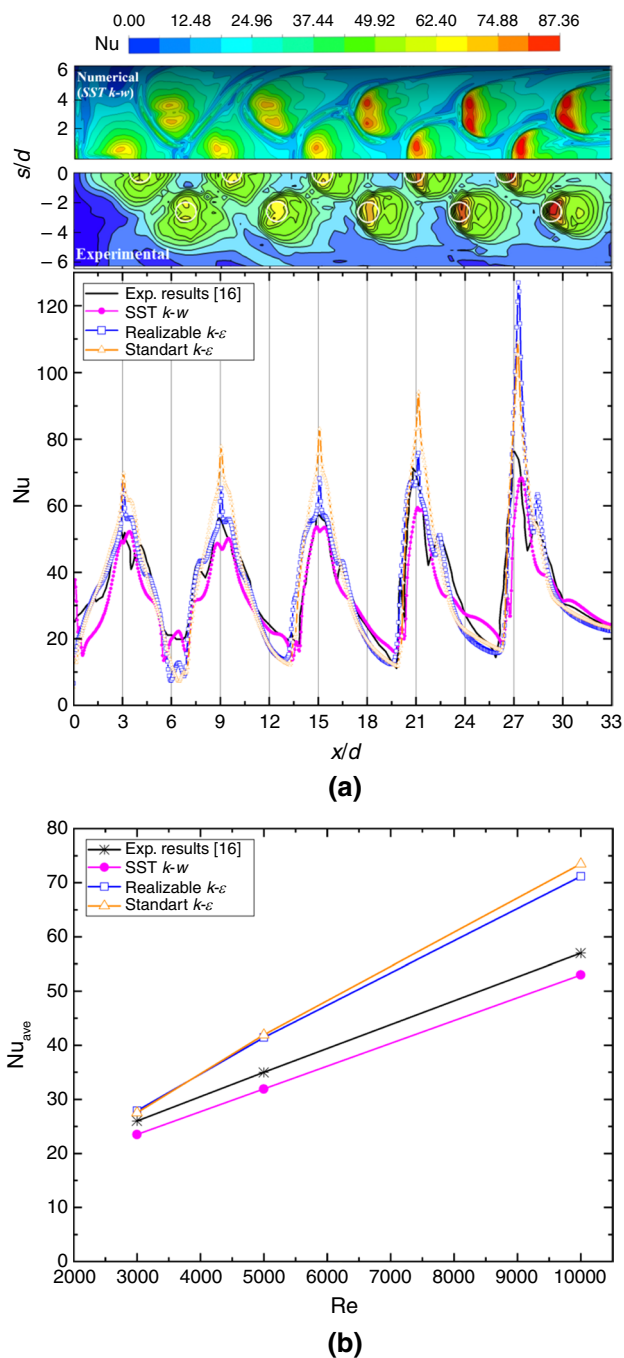


**Fig. 4** Performance evaluation of numerical and experimental results [16] in terms of turbulence models ( $H/d=1.0$  and  $G/d=1.0$ ), **a** contour plot and variation of local  $Nu$  along the axial direction at  $Re=5000$ , and **b** mean  $Nu$  numbers

## Flow features

The fluid's velocity significantly influences the surface heat transfer rate. Increasing fluid motion on the target plate leads to an enhancement of heat transfer between the fluid and the surface. Also, if the fluid velocity increases, it



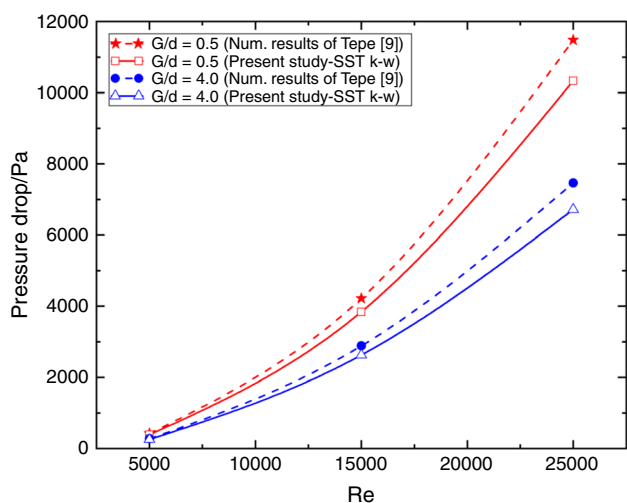


**Fig. 5** Comparison of pressure drops at  $5000 \leq Re \leq 25,000$  for  $H/d = 8.0$  between the present study and the numerical study by Tepe [9]

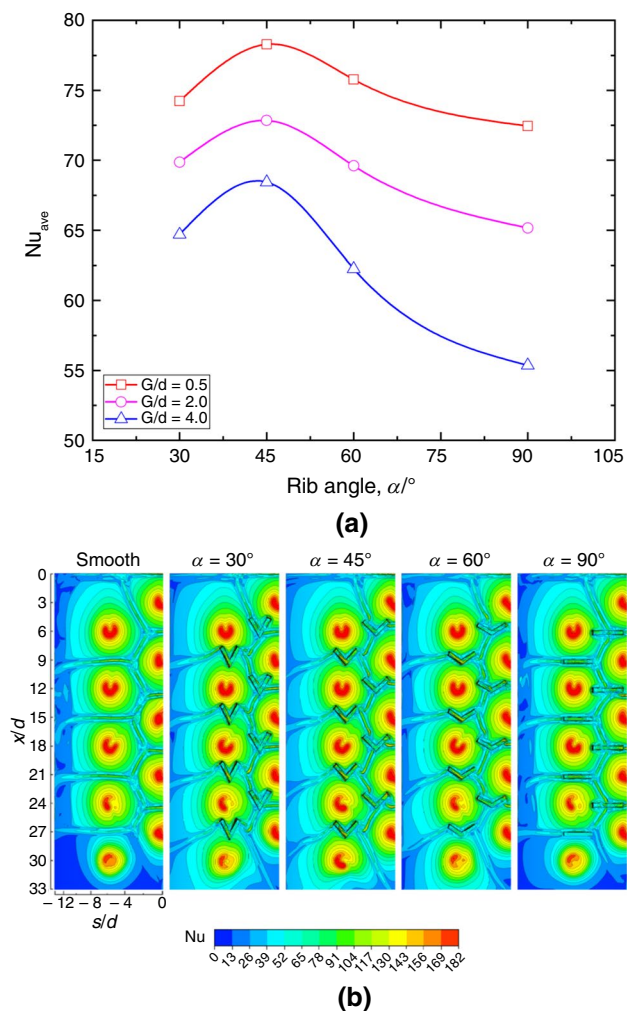


**Fig. 6** Effects of rib angle at  $Re = 25,000$  on **a** variation of mean  $Nu$  number and **b** distribution of local  $Nu$  number

causes the boundary layer thickness to reduce. This can be achieved using different configurations, such as extended jets and rib-roughened surfaces. Surface roughening is a commonly used technique to improve heat transfer by increasing turbulence and disrupting the boundary layer on the relevant surface. Different normalized rib heights ( $H_r/d = 0, 0.2, 0.3,$  and  $0.4$ ) at an angle of  $\alpha = 45^\circ$  were examined to investigate the impact of  $VSR$  height on flow and heat transfer characteristics for various nozzle lengths in this study.

Figure 7 shows the detailed image of the  $Nu$  number dissipation and velocity field near the  $VSR$  at  $x/d = 18.5$  and  $Re = 25,000$ . The results showed that increasing rib height ( $H_r/d > 0.3$ ) reduced flow velocity on the curved surface- $VSR$  intersection region, resulting in diminished heat transfer. Moreover, elongating the nozzle to the measurement region increased heat transfer and the flow velocity at the surface and near the rib. As shown in the figure, the study also revealed that a relatively low  $VSR$  height ( $H_r/d = 0.2$ ) enhanced convective heat transfer, while an improper designing  $VSR$  height ( $H_r/d = 0.4$ ) diminished heat transfer due to the fluid being trapped in the  $VSR$  corner.

In a jet impingement flow, there are typically three regions. The potential core region is the region closest to the nozzle where the fluid is still accelerating and the velocity is highest. In the developing region, the fluid still adjusts to the surrounding conditions, and the velocity gradually decreases. The fully developed region is the region farthest from the nozzle where the fluid has reached a steady state, and the velocity profile is relatively constant [45]. However, if the distance between the nozzle and the target surface is sufficiently high, the stronger cross-flow (perpendicular to the main flow direction) can develop in the conventional ( $G/d = 8.0$ ) cooling duct. This causes the stagnation region to move downstream along the streamwise direction of the plate [46–48]. In this situation, the flow outside the potential core region impinges the concave surface at a lower velocity. Therefore, increasing the distance between the orifice plate (or nozzle) and the target surface or increasing the  $G/d$  ratio significantly in an impinging jet system will decrease the flow rate. It leads to a diminishing in cooling efficiency, accordingly. Moreover, consistent with the literature [6, 38, 49], elongating the injection holes toward the measurement region and locating  $VSRs$  to the surface minimized deflection caused by cross-flow, as illustrated in Fig. 7.

In addition, the leading edge of  $VSRs$  in the cooling channel had higher local  $Nu$  numbers than other parts, such as the top side and trailing edge. The interaction between the elongated impinging jet and  $VSR$  can lead to high-velocity gradients at the leading edge of the ribs. Weak backflow regions and strong velocity fluctuations near the  $VSRs$  can be formed as a result of these high-velocity gradients. These regions can also enhance heat transfer

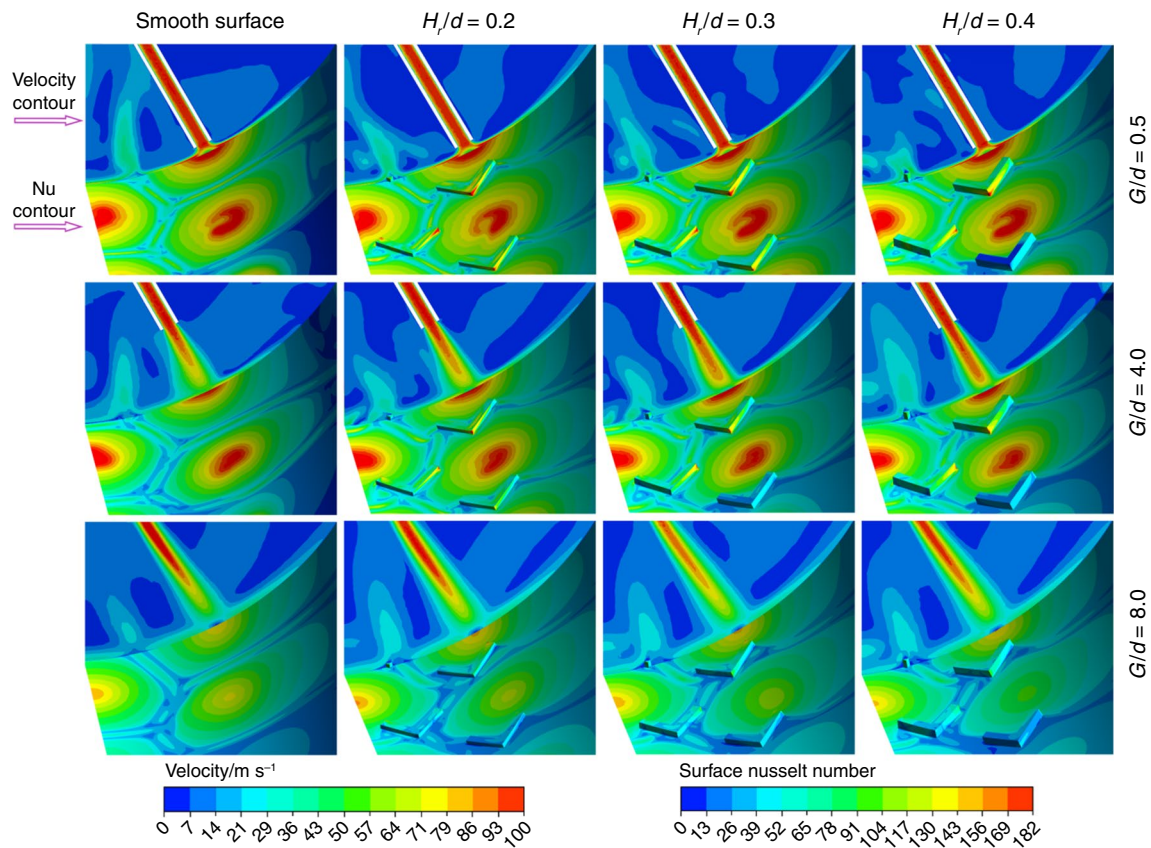


**Fig. 7** Detailed image of the velocity field and  $Nu$  distribution near the VSR at  $x/d = 18.5$  and  $Re = 25,000$

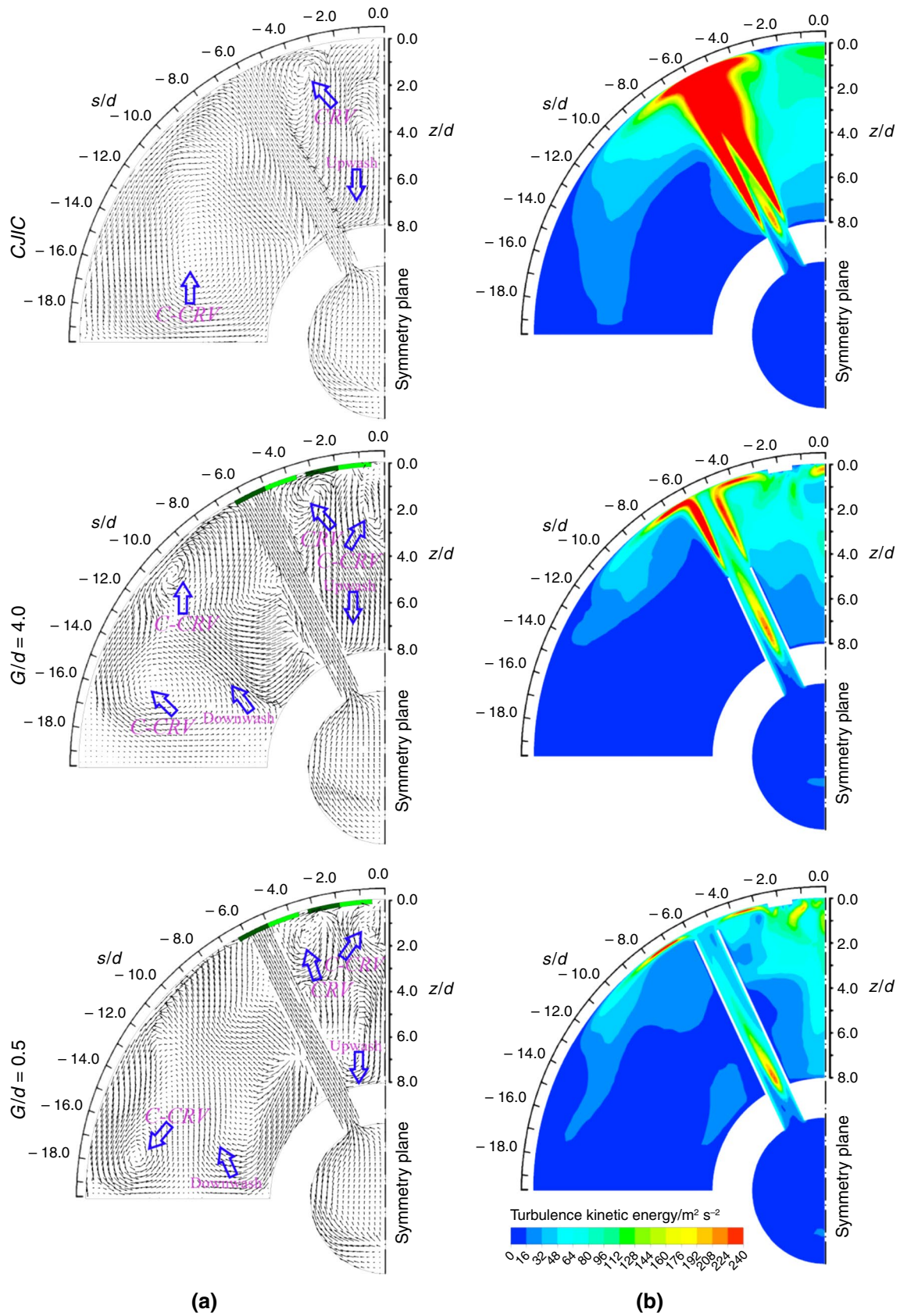
by creating turbulent mixing, which increases total heat transfer and reduces the boundary layer thickness [35].

Figure 8 compares the flow features for conventional (*CJIC*) and elongated jet impingement cooling designs at  $x/d = 24$ ,  $H_r/d = 0.2$ , and  $Re = 25,000$ , including velocity vector fields and turbulent kinetic energy contour plots. As shown in Fig. 8a, the collision between the adjacent jet stream and the wall in all configurations generated a clockwise vortex close to  $s/d \cong -3.5$ . Elongated nozzle holes and ribs also contributed to creating more turbulent flow by forming clockwise rotation (*CRV*) and counter-clockwise rotation (*C-CRV*) vortices near the test region, which maintain a stronger attachment of the fluid to the surface. Besides, downward velocity vectors observed in the proposed models ( $G/d = 0.5$  and  $4.0$  for  $H_r/d = 0.2$ ) were unavailable in the *CJIC*. As illustrated in Fig. 8b, elongated nozzles created a stronger flow of fluid that can more effectively carry heat away from the surface being cooled by transferring the turbulent kinetic energy directly to the relevant surface compared to *CJIC*. *VSRs* also helped to improve the uniformity

of the heat transfer by providing more process fluid to areas that may have been previously under-cooled. This also led to an increase in the area-averaged  $Nu$  number.

### Average $Nu$ numbers

This study aims to elucidate the combination of elongated nozzles and ribs to augment the heat transfer efficiency of the curved surface and investigate how these modifications affect total heat transfer. The study explains how the  $Nu$  number changes on *VSR*-roughened surfaces for various parameters, including  $Re$  number, normalized rib height, and normalized injection holes to target surface distance, as shown in Fig. 9. Numerical results suggested that heat transfer was enhanced by increasing the rib height to  $H_r/d = 0.2$  and extending the injection holes to the target surface. However, the dimensionless rib height above  $0.2$  for all  $Re$  numbers has a negative effect on the mean  $Nu$  number, as illustrated in the figure.



**Fig. 8** Comparison of the flow features for conventional (*CJIC* and elongated jet impingement cooling designs at  $x/d=24$ ,  $H_i/d=0.2$ , and  $Re=25,000$ ; **(a)** velocity vector field, **(b)** turbulent kinetic energy contour plot



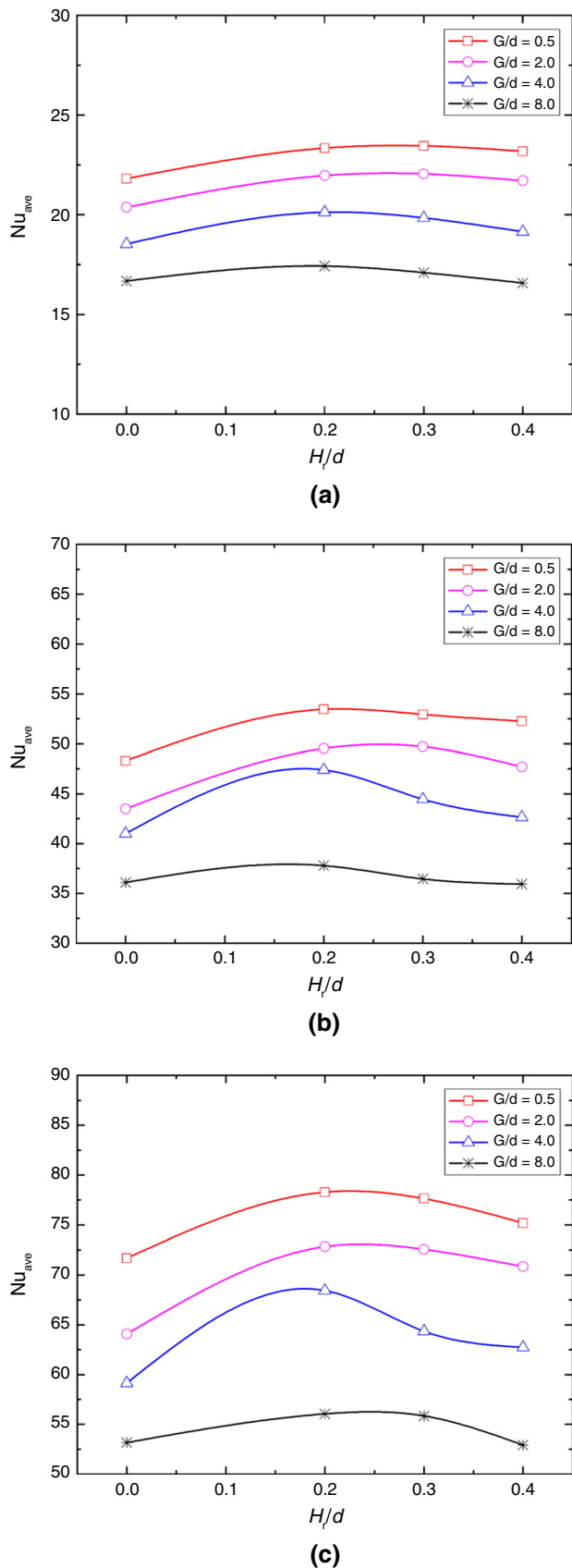


**Fig. 9** Impact of  $G/d$  and  $H_r/d$  for  $\alpha = 45^\circ$  on the variation of mean  $Nu$  numbers at **a**  $Re = 5000$ , **b**  $Re = 15,000$ , **c**  $Re = 25,000$

It was found that locating the V-shaped ribs on the stagnation regions, which form due to the interaction between adjacent jets, improved overall heat transfer. For instance, on a smooth concave surface at  $Re = 25,000$  and  $G/d = 4.0$ , the average  $Nu$  number was 59.15. However, on the rib-roughened target surface ( $H_r/d = 0.2$ ), it increased by 15.70% to 68.44. Also, the mean  $Nu$  number was 53.16 in a conventional impinging model with a smooth surface at  $Re = 25,000$ . The average  $Nu$  number increased by 47.23% to 78.28 for  $G/d = 0.5$  and  $H_r/d = 0.2$  under the same flow conditions on the rib-roughened model. Similar results were observed for the other  $Re$  numbers and nozzle lengths investigated. For example, on a smooth curved surface at  $Re = 15,000$  and  $G/d = 2.0$ , the mean  $Nu$  number was 43.47. On the other hand, it increased on the VSR-roughened surface for  $H_r/d = 0.2$  by 13.90% to 49.52. Furthermore, the mean  $Nu$  number was 38.69 in a CJIC scheme with a smooth surface at  $Re = 15,000$ . The area-averaged  $Nu$  number increased by 38.14% to 53.44 for  $G/d = 0.5$  and  $H_r/d = 0.2$  with identical flow conditions. Because assembling ribs on a concave surface causes turbulence and disrupts the thermal boundary layer, which increases heat transfer in the measurement region.

However, while the average  $Nu$  number is 53.16 for  $Re = 25,000$  in the CJIC model, this value is 56.15 on the VSR-roughened surface. In this case, an increase of 5.6% was calculated. This is due to the relatively high distance between the orifice surface and the measurement region ( $H/d = 8.0$ ) in the absence of elongated jet holes. Overall, the study demonstrated that combining elongated jet holes and ribs can significantly enhance heat transfer performance on a curved surface. It's worth noting that these findings are specific to the particular study, and the results may vary depending on the specific conditions and geometries of the jet impingement cooling system. However, these dimensionless parameters can be used to optimize the design of jet impingement cooling systems for concave surfaces and improve heat transfer performance by adjusting the rib height and nozzle length.

### Local heat transfer

In typical jet-impingement cooling, the flow at high velocity is directed through a hole or slot in the impingement plate. After impinging on the target surface, it changes direction and discharges along the flow direction. Cross-flow created by this situation can affect the system's heat and flow characteristics. As subsequent jet flows are added, the cross-flow velocity gradually augments toward the main flow direction. This effect is more pronounced in designs with a large spacing between the nozzle and the target surface, as the fluid travels longer before reaching the surface. The longer travel distance means the fluid is more likely to be



affected by the cross-flow and lose momentum, leading to a weaker impingement force by tilting the jet flow and lower heat transfer efficiency. Therefore, the combination of elongated jet holes and ribs may mitigate the adverse effects of cross-flow.

Contour plots of  $Nu$  number distributions for different  $G/d$  and  $H_r/d$  ratios for  $\alpha=45^\circ$  at  $Re=25,000$  are shown in Fig. 10. It can be seen that decreasing  $G/d$  significantly contributes to heat transfer, particularly in the stagnation regions. In addition, the contribution of the presence of extended jets was relatively low in the spanwise direction and last jet region ( $x/d \geq 27$ ) for the local  $Nu$  distribution. Because the orifice surface-target surface distance ( $H$ ) was too large, the cross-flow effect became dominant, and the system's overall efficiency was reduced, especially in the last jet region [49]. On the contrary, a significant increase in local heat transfer dissipation was observed in the wall jet regions, particularly in the last region, with the installation of V-shaped ribs on the measurement region. The heat transfer area is more spread toward the wall jet region and streamwise direction on the rib-roughened surfaces than on the smooth surface. However, it is seen in the figure that the relatively high normalized  $VSR$  height ( $H_r/d=0.4$ ) had an adverse effect on local heat transfer distribution. Overall, the results suggest that using extended jets and  $VSRs$  together can effectively enhance heat transfer uniformity on a curved surface.

Laterally averaged  $Nu$  distributions on the target surface at  $H_r/d=0.2$  are shown for different  $Re$  numbers in Fig. 11, where the letters  $S$  and  $R$  denote smooth and roughened surfaces, respectively. Furthermore, the figure includes the results of the conventional jet impingement cooling scheme to facilitate a comparison with the proposed models. Due to the jet interaction and cross-flow, heat transfer in the final jet region of the  $CJIC$  scheme ( $x/d \geq 27$ ) has decreased. The impact of elongated jets on heat transfer is evident for smooth and ribbed surfaces across all  $Re$  numbers. Additionally, mounting ribs on the surface decreased the uneven local heat transfer distribution along both the flow and lateral directions in the cooling duct. It is found that locating the V-shaped ribs on dead flow zones of the curved surface enhanced heat transfer, particularly for the final region. As given in the figure, the optimal  $H_r/d$  and  $G/d$  ratios increase convective heat transfer on  $VSR$ -roughened concave surfaces and minimize the mutual impact of cross-flow when compared to the  $CJIC$ , consistent with the literature [38, 48].

Furthermore, non-uniform heat transfer distribution can result in uneven thermal expansion and contraction of the material, leading to internal stresses within the material that can cause it to deform or even fail over time. It can also lead to areas of stagnant fluid flow, where the fluid is

not effectively removing heat from the surface. This can lead to overheating and accelerated material degradation in those areas. In this regard, ensuring uniform heat transfer at the target surface as much as possible is essential. In other words, the simultaneous use of extended jet holes (especially at decreasing  $G/d$  ratios) and ribs reduces the formation of dead flow zones, providing a relatively more uniform dissipation on the curved surface and also increasing the efficiency of the last jets.

### Thermal performance criterion

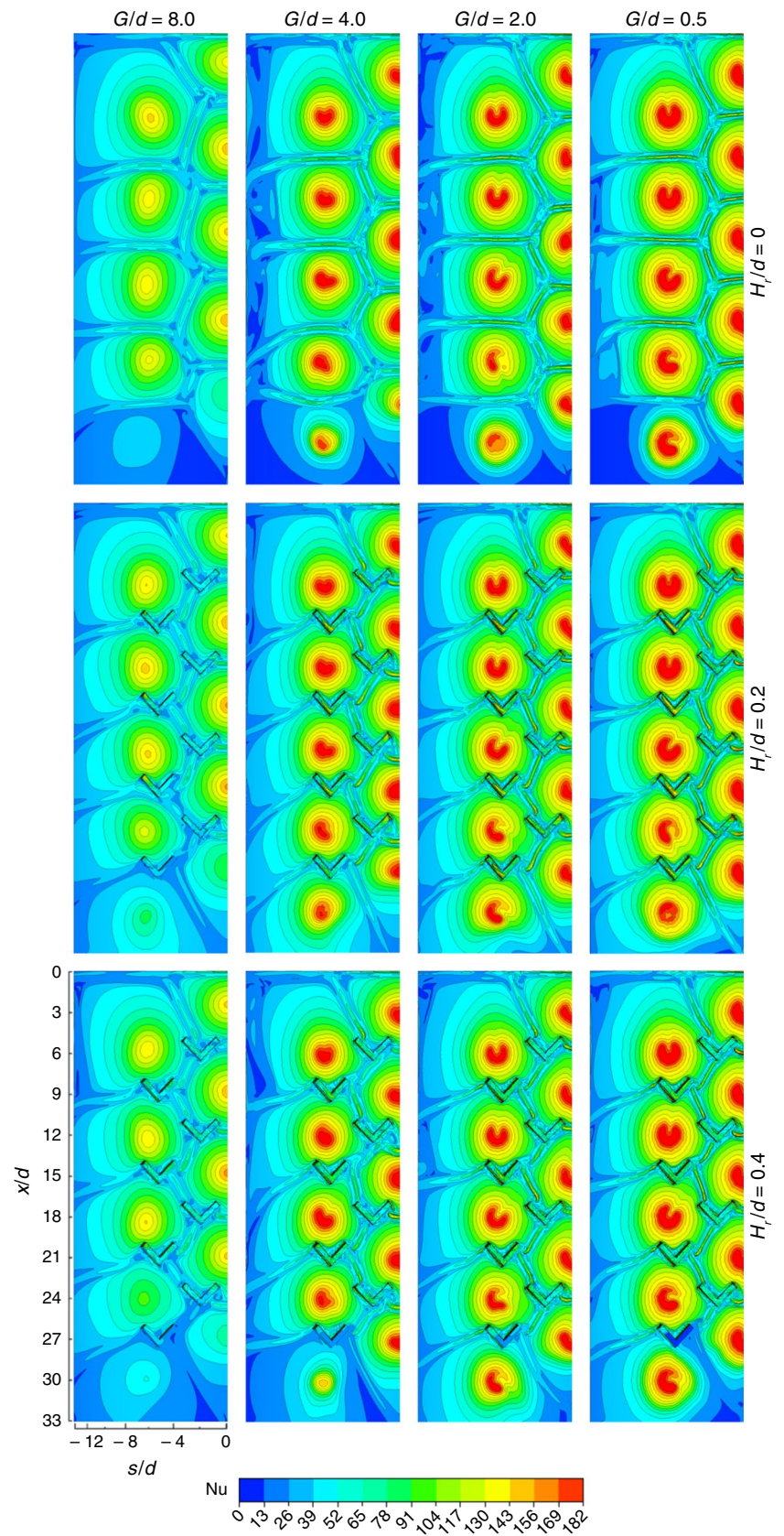
$TPC$  analysis is a commonly used method in heat transfer to investigate the effectiveness of impingement cooling on surfaces with varying roughness or topology. However, it is important to consider that these modifications can also adversely affect the pumping power by increasing pressure drop for an optimal cooling duct design. The  $TPC$  analysis determines if elongated injection holes are feasible for cooling rib-roughened curved surfaces in this study. As a result of this analysis, if the  $TPC$  number is more than 1, the heat transfer enhancement is higher than the increase in compressor work owing to the pressure drop. It can also be expressed, shown in Eq. (12), as a function of the friction factor ( $f$ ) and the area-averaged  $Nu$  number [50, 51].

$$TPC = \left( \frac{\overline{Nu}_r}{\overline{Nu}_s} \right) / \left( \frac{f_r}{f_s} \right)^{-1/3} \quad (12)$$

where the variables are related to two different configurations of jet impingement: a staggered conventional jet array with a smooth curved surface (represented by  $f_s$  and  $\overline{Nu}_s$ ) and a staggered elongated jet array with a rib-roughened curved surface (symbolized by  $f_r$  and  $\overline{Nu}_r$ ).

When designing an impinging jet cooling scheme, it is crucial to consider the balance between heat transfer efficiency and pressure drop. By evaluating  $TPC$  for  $0.2 \leq H_r/d \leq 0.4$  ( $\alpha=45^\circ$ ) and  $0.5 \leq G/d \leq 8.0$ , whether the existing together of the elongated nozzles and  $VSRs$  is an effective method in jet impingement cooling scheme for the curved surface was determined, as in Fig. 12. The numerical results show that the proposed modifications have negligibly boosted pressure drops as well as the heat transfer efficiency of the system. The figure illustrates that  $TPC$  values increase with increasing  $Re$  number for suggested models. According to the  $TPC$ , the physical models are feasible at  $H_r/d=0.2$  for enhancing convective heat transfer except for  $G/d=8.0$  at  $Re=5000$  on a  $VSR$ -roughened surface. However,  $H_r/d=0.4$  is not a feasible design for enhancement heat transfer for relatively all patterns. Besides,  $TPCs$  are maximum at  $G/d=2.0$  for investigated jet plate-measurement region distance.

**Fig. 10** Contour plots of  $Nu$  number distributions for different  $G/d$  and  $H/d$  ratios at  $Re=25,000$



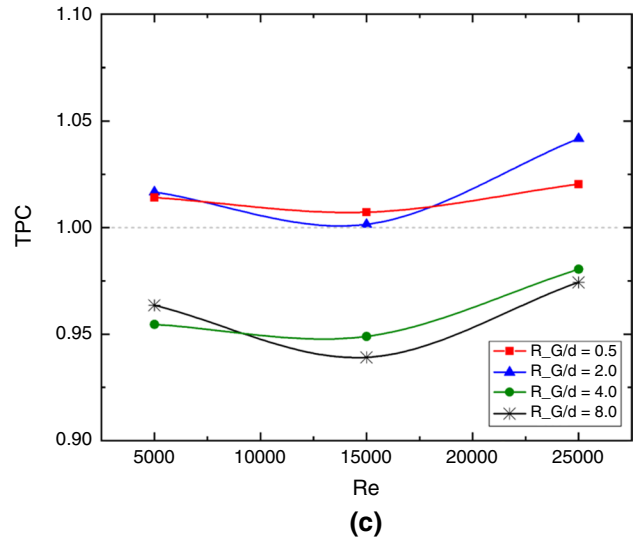
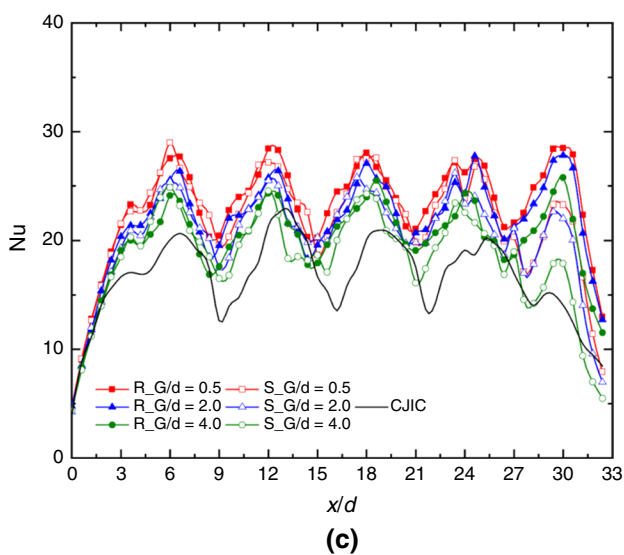
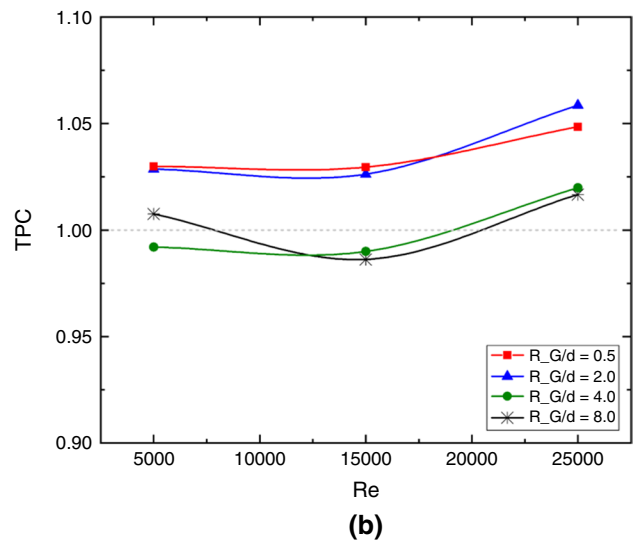
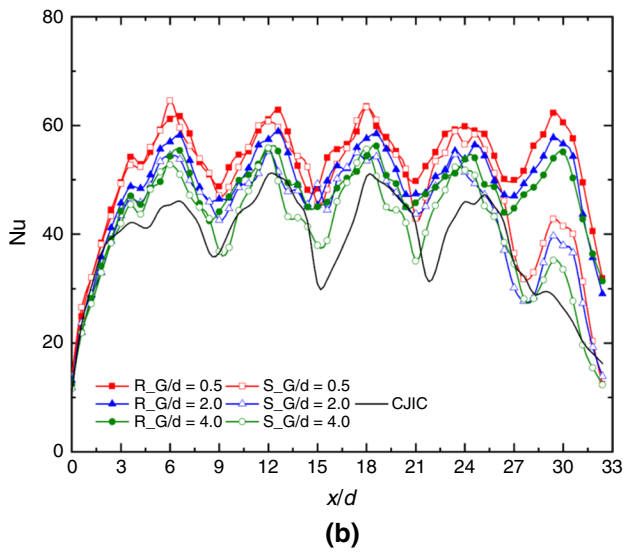
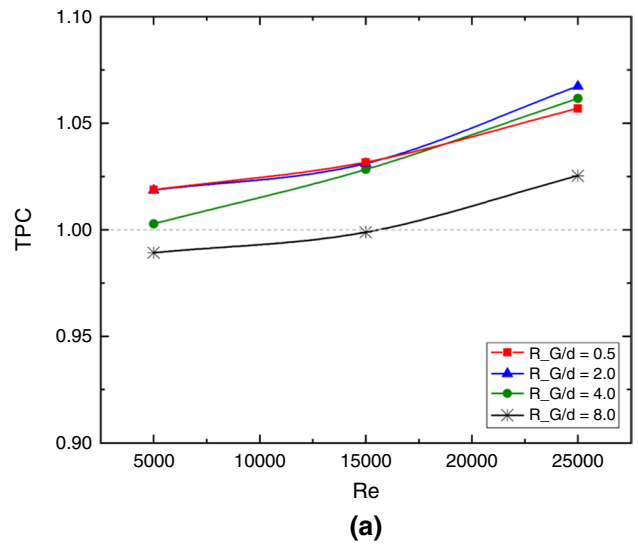
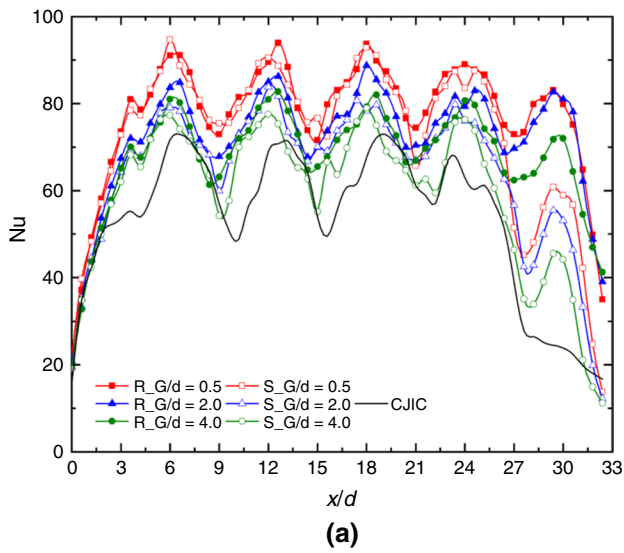


Fig. 11 Laterally averaged  $Nu$  number distributions on smooth and ribbed surfaces at  $H_r/d=0.2$  for **a**  $Re=25,000$ , **b**  $Re=15,000$ , **c**  $Re=5000$

Fig. 12 Evaluation of  $TPC$  on rib-roughened curved surfaces with different injection holes for **a**  $H_r/d=0.2$ , **b**  $H_r/d=0.3$ , **c**  $H_r/d=0.4$



## Conclusions

The present study aims to elucidate numerically how elongated jet holes on a rib-roughened curved surface affect heat and flow features in a staggered array jet impingement configuration. For this reason, the effect of different normalized injection hole-to-test plate distances ( $G/d$ ), normalized rib heights ( $H_r/d$ ), rib angles ( $\alpha$ ), and Re numbers on smooth and ribbed surfaces' convective heat transfer performance was examined. With this goal in mind, the current study thoroughly investigated several key parameters, including local and area-averaged  $Nu$  numbers, velocity vector plots, velocity contours, turbulence kinetic energies, and  $TPCs$ . According to the numerical results, the  $SST k-\omega$  model in ANSYS Fluent could model the complicated flow region with reasonable accuracy and correctly capture the staggered array jet-crossflow interaction. As a result, both local and averaged heat transfer data predicted by the solution procedure agreed well with the experimental and numerical results in the literature. This investigation yielded several important results, as follows.

- According to the evaluation of  $TPC$ , the coexistence of elongated injection holes and ribs in a staggered array of impinging jets on a curved surface was feasible, particularly  $G/d \leq 2.0$ , for enhancing overall heat transfer since the increase in heat transfer was more distinct than the rise in pressure loss.
- Mounting ribs to the relevant surface led to a significant enhancement in heat transfer performance, especially at a rib angle of  $\alpha = 45^\circ$ , compared to the case in the conventional jet-impinging design (without elongated jet holes and ribs). This improvement is attributed to the increased flow interaction and turbulence intensity near the surface. Additionally, the results indicated that the flow field near the surface becomes more complex with ribs due to the formation of secondary vortices, which can further enhance heat transfer. For example, heat transfer has been increased by 15.70% by just locating ribs compared to a smooth surface at  $G/d = 8.0$  and  $Re = 25,000$ . Moreover, using a combination of elongated holes and ribs, the highest heat transfer augmentation was determined as 47.23% (at  $H_r/d = 0.2$ ) at  $Re = 25,000$  when the  $G/d$  decreased by 0.5.
- Numerical results indicate that stagnation regions are formed where the jet stream impinging the surface comes across the adjacent jets while flowing from the wall jet region, adversely affecting the heat transfer correspondingly. However, with the addition of ribs to these areas, stagnation regions are disturbed. As a result, relatively more uniform distribution and an increase in heat transfer are provided.

Although this study provides valuable insights into the effect of extended nozzles on heat transfer and flow characteristics in a staggered array jet impingement configuration on a rib-roughened curved surface, these findings can also aid in the design and optimization of cooling systems for various engineering applications.

**Author contributions** All authors contributed to the study. OY and UD contributed to conceptualization, visualization, supervision, and writing review and editing; OY contributed to methodology; OY and UD contributed to software; OY and UD contributed to validation project administration. OY contributed to formal analysis, original manuscript writing, and data curation; OY contributed to the investigation and resources. All authors read and approved the final manuscript.

**Funding** Open access funding provided by the Scientific and Technological Research Council of Türkiye (TÜBİTAK).

**Data availability** All data are available in the manuscript.

## Declarations

**Conflict of interest** The authors do not have any conflict of interest.

**Open Access** This article is licensed under a Creative Commons Attribution 4.0 International License, which permits use, sharing, adaptation, distribution and reproduction in any medium or format, as long as you give appropriate credit to the original author(s) and the source, provide a link to the Creative Commons licence, and indicate if changes were made. The images or other third party material in this article are included in the article's Creative Commons licence, unless indicated otherwise in a credit line to the material. If material is not included in the article's Creative Commons licence and your intended use is not permitted by statutory regulation or exceeds the permitted use, you will need to obtain permission directly from the copyright holder. To view a copy of this licence, visit <http://creativecommons.org/licenses/by/4.0/>.

## References

1. Lee CH, Lim KB, Lee SH, Yoon YJ, Sung NW. A study of the heat transfer characteristics of turbulent round jet impinging on an inclined concave surface using liquid crystal transient method. *Exp Therm Fluid Sci.* 2007;31:559–65. <https://doi.org/10.1016/j.expthermflusci.2006.06.004>.
2. Yalçinkaya O, Durmaz U, Tepe AÜ, Uysal Ü, Özel MB. Effect of slot-shaped pins on heat transfer performance in the extended jet impingement cooling. *Int J Therm Sci.* 2022;179: 107698. <https://doi.org/10.1016/j.ijthermalsci.2022.107698>.
3. Yalçinkaya O, Durmaz U, Tepe AÜ, Uysal Ü, Özel MB. Assessment of convective heat transfer characteristics for elliptical-shaped pin-roughened surface for the jet impingement cooling. *ASME J Heat Mass Transf.* 2023;145:1–11. <https://doi.org/10.1115/1.4055940>.
4. Pazarlıoğlu HK, Tepe AÜ, Tekir M, Arslan K. Effect of new design of elongated jet hole on thermal efficiency of solar air heater. *Therm Sci Eng Prog.* 2022;36: 101483. <https://doi.org/10.1016/j.tsep.2022.101483>.
5. Fenot M, Vullierme JJ, Dorignac E. Local heat transfer due to several configurations of circular air jets impinging on a flat plate with and without semi-confinement. *Int J Therm Sci.*



- 2005;44:665–75. <https://doi.org/10.1016/j.ijthermalsci.2004.12.002>.
6. Tepe AÜ, Yetişken Y, Uysal Ü, Arslan K. Experimental and numerical investigation of jet impingement cooling using extended jet holes. *Int J Heat Mass Transf.* 2020;158:119945. <https://doi.org/10.1016/j.ijheatmasstransfer.2020.119945>.
  7. Ekkad SV, Esposito EI, Kim YW. (2008) Zero-cross-flow impingement via an array of differing length, extended ports, Patent Application Publication (10) Pub. No.: US20080271458A1. <https://patents.google.com/patent/US20080271458A1/en>.
  8. Yong S, Zhang JZ, Xie GN. Convective heat transfer for multiple rows of impinging air jets with small jet-to-jet spacing in a semi-confined channel. *Int J Heat Mass Transf.* 2015;86:832–42. <https://doi.org/10.1016/j.ijheatmasstransfer.2015.03.073>.
  9. Tepe AÜ. Numerical investigation of a novel jet hole design for staggered array jet impingement cooling on a semicircular concave surface. *Int J Therm Sci.* 2021;162: 106792. <https://doi.org/10.1016/j.ijthermalsci.2020.106792>.
  10. Demir F, Turgut O, Calisir T. Investigation of swirling impinging jet at low nozzle to plate distances. *J Therm Anal Calorim.* 2023;148:11999–2016. <https://doi.org/10.1007/s10973-023-12484-8>.
  11. El-Wafa AA, Attalla M, Shmroukh AN, Maghrabie HM. Heat transfer of movable air jet impingement over flat plate: experimental implementation. *J Therm Anal Calorim.* 2023;148:13393–412. <https://doi.org/10.1007/s10973-023-12656-6>.
  12. Fenot M, Dorignac E, Vullierme JJ. An experimental study on hot round jets impinging a concave surface. *Int J Heat Fluid Flow.* 2008;29:945–56. <https://doi.org/10.1016/j.ijheatfluidflow.2008.03.015>.
  13. Lyu Y, Zhang J, Liu X, Shan Y. Experimental study of single-row chevron-jet impingement heat transfer on concave surfaces with different curvatures. *Chinese J Aeronaut.* 2019;32:2275–85. <https://doi.org/10.1016/j.cja.2019.07.002>.
  14. Yang B, Chang S, Wu H, Zhao Y, Leng M. Experimental and numerical investigation of heat transfer in an array of impingement jets on a concave surface. *Appl Therm Eng.* 2017;127:473–83. <https://doi.org/10.1016/j.applthermaleng.2017.07.190>.
  15. Jung EY, Park CU, Lee DH, Kim KM, Woo TK, Cho HH. Heat transfer characteristics of an angled array impinging jet on a concave duct. *Proc ASME Turbo Expo.* 2012;4:601–7. <https://doi.org/10.1115/GT2012-69566>.
  16. Jung EY, Park CU, Lee DH, Kim KM, Cho HH. Effect of the injection angle on local heat transfer in a showerhead cooling with array impingement jets. *Int J Therm Sci.* 2018;124:344–55. <https://doi.org/10.1016/j.ijthermalsci.2017.10.033>.
  17. Heo MW, Lee KD, Kim KY. Parametric study and optimization of staggered inclined impinging jets on a concave surface for heat transfer augmentation. *Numer Heat Transf Part A Appl.* 2012;61:442–62. <https://doi.org/10.1080/10407782.2012.654453>.
  18. Qiu D, Wang C, Luo L, Wang S, Zhao Z, Wang Z. On heat transfer and flow characteristics of jets impinging onto a concave surface with varying jet arrangements. *J Therm Anal Calorim.* 2020;141:57–68. <https://doi.org/10.1007/s10973-019-08901-6>.
  19. Tan L, Zhang JZ, Xu HS. Jet impingement on a rib-roughened wall inside semi-confined channel. *Int J Therm Sci.* 2014;86:210–8. <https://doi.org/10.1016/j.ijthermalsci.2014.06.037>.
  20. Tong F, Gou W, Zhao Z, Gao W, Li H, Li L. Numerical investigation of impingement heat transfer on smooth and roughened surfaces in a high-pressure turbine inner casing. *Int J Therm Sci.* 2020;149: 106186. <https://doi.org/10.1016/j.ijthermalsci.2019.106186>.
  21. Caliskan S. Flow and heat transfer characteristics of transverse perforated ribs under impingement jets. *Int J Heat Mass Transf.* 2013;66:244–60. <https://doi.org/10.1016/j.ijheatmasstransfer.2013.07.027>.
  22. Xie G, Liu X, Yan H, Qin J. Turbulent flow characteristics and heat transfer enhancement in a square channel with various crescent ribs on one wall. *Int J Heat Mass Transf.* 2017;115:283–95. <https://doi.org/10.1016/j.ijheatmasstransfer.2017.07.012>.
  23. Bai W, Chen W, Yang L, Chyu MK. Numerical investigation on heat transfer and pressure drop of pin-fin array under the influence of rib turbulators induced vortices. *Int J Heat Mass Transf.* 2019;129:735–45. <https://doi.org/10.1016/j.ijheatmasstransfer.2018.10.022>.
  24. Hadipour A, Rajabi Zargarabadi M, Dehghan M. Effect of micro-pin characteristics on flow and heat transfer by a circular jet impinging to the flat surface. *J Therm Anal Calorim.* 2020;140:943–51. <https://doi.org/10.1007/s10973-019-09232-2>.
  25. Kannan BT, Sundararaj S. Steady state jet impingement heat transfer from axisymmetric plates with and without grooves. *Procedia Eng.* 2015;127:25–32. <https://doi.org/10.1016/j.proeng.2015.11.320>.
  26. van Hout R, Rinsky V, Sasson N, Hershovich C, Tshuva M, Grobman YJ. Axisymmetric jet impingement on a dimpled surface: effect of impingement location on flow field characteristics. *Int J Heat Fluid Flow.* 2018;74:53–64. <https://doi.org/10.1016/j.ijheatfluidflow.2018.09.010>.
  27. Sriromreun P, Sriromreun P. Experimental and numerical studies of heat transfer characteristics for impinging jet on dimple surfaces. *Chem Eng Trans.* 2018;70:1273–8. <https://doi.org/10.3303/CET1870213>.
  28. Gan T, Ming T, Fang W, Liu Y, Miao L, Ren K, et al. Heat transfer enhancement of a microchannel heat sink with the combination of impinging jets, dimples, and side outlets. *J Therm Anal Calorim.* 2020;141:45–56. <https://doi.org/10.1007/s10973-019-08754-z>.
  29. Eiamsa-ard S, Phila A, Thianpong C, Chuwattanakul V, Maruyama N, Hirota M. Enhanced heat transfer performance in channel with delta-wing perforated V-type baffles. *J Therm Anal Calorim.* 2023;148:11283–301. <https://doi.org/10.1007/s10973-023-12452-2>.
  30. Singh TP, Dewan A. Improvement in cooling using a sinusoidal wavy surface for a turbulent dual jet: a computational study. *J Therm Anal Calorim.* 2023;148:2935–47. <https://doi.org/10.1007/s10973-022-11695-9>.
  31. Monfared RH, Niknejadi M, Toghraie D, Barnoon P. Numerical investigation of swirling flow and heat transfer of a nanofluid in a tube with helical ribs using a two-phase model. *J Therm Anal Calorim.* 2022;147:3403–16. <https://doi.org/10.1007/s10973-021-10661-1>.
  32. Farahani SD, Hajian E. Achieving uniform heat transfer coefficient in coaxial pulsating jet. *J Therm Anal Calorim.* 2022;147:2833–46. <https://doi.org/10.1007/s10973-021-10582-z>.
  33. Yan WM, Liu HC, Soong CY, Yang WJ. Experimental study of impinging heat transfer along rib-roughened walls by using transient liquid crystal technique. *Int J Heat Mass Transf.* 2005;48:2420–8. <https://doi.org/10.1016/j.ijheatfluidflow.2008.05.003>.
  34. Katti V, Prabhu SV. Heat transfer enhancement on a flat surface with axisymmetric detached ribs by normal impingement of circular air jet. *Int J Heat Fluid Flow.* 2008;29:1279–94. <https://doi.org/10.1016/j.ijheatfluidflow.2008.05.003>.
  35. Caliskan S, Baskaya S. Velocity field and turbulence effects on heat transfer characteristics from surfaces with V-shaped ribs. *Int J Heat Mass Transf.* 2012;55:6260–77. <https://doi.org/10.1016/j.ijheatmasstransfer.2012.06.056>.
  36. Caliskan S, Baskaya S. Experimental investigation of impinging jet array heat transfer from a surface with V-shaped and convergent-divergent ribs. *Int J Therm Sci.* 2012;59:234–46. <https://doi.org/10.1016/j.ijthermalsci.2012.04.013>.

37. Rasheed A, Allauddin U, Ali HM, Uzair M, Verdin PG, Siddiqui YH. Heat transfer and fluid flow characteristics investigation using detached ribs in an axisymmetric impinging jet flow. *J Therm Anal Calorim.* 2022;147:14517–37. <https://doi.org/10.1007/s10973-022-11640-w>.
38. Tepe AÜ, Uysal Ü, Yetişken Y, Arslan K. Jet impingement cooling on a rib-roughened surface using extended jet holes. *Appl Therm Eng.* 2020;178:115601. <https://doi.org/10.1016/j.applthermaleng.2020.115601>.
39. Wilcox DC. Reassessment of the scale-determining equation for advanced turbulence models. *AIAA J.* 1988;26:1299–310. <https://doi.org/10.2514/3.10041>.
40. Menter FR. Two-equation eddy-viscosity turbulence models for engineering applications. *AIAA J.* 1994;32:1598–605. <https://doi.org/10.2514/3.12149>.
41. Wang T, Lin M, Bunker RS. Flow and heat transfer of confined impingement jets cooling using a 3-D transient liquid crystal scheme. *Int J Heat Mass Transf.* 2005;48:4887–903. <https://doi.org/10.1016/j.ijheatmasstransfer.2005.04.020>.
42. Bergman TL, Lavine AS, Incropera FP, Dewitt DP. *Fundamentals of Heat and Mass Transfer.* 7th ed. John Wiley & Sons, Inc.; 2011.
43. Richardson LF, Gaunt JA. The deferred approach to the limit. part i. single lattice. part ii. interpenetrating lattices. *Philos Trans R Soc Math Phys Character.* 1927;226:299–361. <https://doi.org/10.1098/rsta.1927.0008>.
44. Boache PJ. Perspective: a method for uniform reporting of grid refinement studies. *J Fluids Eng Trans ASME.* 1994;116:405–13. <https://doi.org/10.1115/1.2910291>.
45. Viskanta R. Nusselt-Reynolds prize paper heat transfer to impinging isothermal gas and flame jets. *Exp Therm Fluid Sci.* 1993;6:111–34. [https://doi.org/10.1016/0894-1777\(93\)90022-B](https://doi.org/10.1016/0894-1777(93)90022-B).
46. Kim T, Jung EY, Bang M, Lee C, Moon HK, Cho HH. Heat transfer measurements for array jet impingement with castellated wall. *J Turbomachinery.* 2021;144(3):031009. <https://doi.org/10.1115/GT2021-58895>.
47. Behbahani AI, Goldstein RJ. Local heat transfer to staggered arrays of impinging circular air jets. In: *Turbo Expo: Power for Land, Sea, and Air 1982* (Vol. 79597, p. V004T09A016). American Society of Mechanical Engineers. <https://doi.org/10.1115/1.3227423>.
48. Rhee DH, Choi JH, Cho HH. Flow and heat (mass) transfer characteristics in an impingement/effusion cooling system with cross-flow. *J Turbomach.* 2003;125:74–82. <https://doi.org/10.1115/1.1519835>.
49. Tepe AÜ, Arslan K, Yetişken Y, Uysal Ü. Effects of extended jet holes to heat transfer and flow characteristics of the jet impingement cooling. *J Heat Transfer.* 2019;141:1–14. <https://doi.org/10.1115/1.4043893>.
50. Maradiya C, Vadher J, Agarwal R. The heat transfer enhancement techniques and their thermal performance factor. *Beni-Suef Univ J Basic Appl Sci.* 2018;7:1–21. <https://doi.org/10.1016/j.bjbas.2017.10.001>.
51. Chang SW, Chiang PA, Cai WL. Thermal performance of impinging jet-row onto trapezoidal channel with different effusion and discharge conditions. *Int J Therm Sci.* 2021;159: 106590. <https://doi.org/10.1016/j.ijthermalsci.2020.106590>.

**Publisher's Note** Springer Nature remains neutral with regard to jurisdictional claims in published maps and institutional affiliations.